Pergamon

Atmospheric Environment Vol. 31, No. 13, pp. 2011–2022, 1997

PII: S1352-2310(97)00281-6
1352-2310/97 $17.00 + 0.00

OBSERVATIONS OF JETS IN DENSITY STRATIFIED CROSSFLOWS

PABLO HUQ

College of Marine Studies and Center of Applied Coastal Research, University of Delaware, Newark, Delaware 19716, U.S.A.

(*First received* 3 *April* 1996 *and in final form* 19 *August* 1996. *Published April* 1997)

Abstract—The results are presented of a water tunnel study undertaken to determine the characteristics of a circular jet in a density stratified crossflow. Flow visualization indicates that the salient characteristics include a stable potential core of length L in the vicinity of the jet exit. The length of the stable potential core depends on the velocity ratio $\alpha = U_J/U_\infty$ and the non-dimensional frequency ND/U_∞. As α increases the value of L increases; L also increases for increasing values of ND/U_∞ for values of $ND/U_\infty < 0.03$. However, L decreases with increasing ND/U_∞ for values of $ND/U_\infty > 0.03$. Knowledge of this variability is necessary for quantifying mixing rates. Further downwind, the jet trajectory evolves to a maximum height of rise, z_m, and subsequently relaxes to a lower equilibrium level, z_e. Values of z_m and z_e are in agreement with the predictions of scaling arguments. Mean density measurements indicate rapid increase of dilution for small distances from the jet exit; however, for large distances predominantly horizontal mixing processes result in much slower increase of dilution with distance. © 1997 Elsevier Science Ltd.

Key word index: Atmospheric dispersion, lab modelling, density stratification, plumes in crossflow.

1. INTRODUCTION

The flow field of a jet in a crossflow occurs frequently in both environmental and industrial flows and so has been much studied (Fric and Roshko, 1994; Eiff *et al.*, 1995). Flow arising from a chimney stack discharge to the atmosphere, or injection cooling of hot combustion gases in combustors are examples of a jet in a crossflow. The stability of the jet and the location of onset of instability is central in determining rates of entrainment and mixing. In the absence of density variations (i.e. identical jet and crossflow density) it is known that in the immediate vicinity of the jet exit the jet diameter is similar in magnitude to the pipe exit diameter. This region is termed the potential core: here, the streamlines are parallel to the jet axis and the flow is stable, and rates of entrainment and mixing are negligible. The length of the potential core depends on the velocity ratio $\alpha = U_J/U_\infty$ of the jet exit velocity U_J to crossflow velocity U_∞, and is typically about 6 pipe diameters (Rajaratnam, 1976). Beyond the potential core the jet becomes unstable and the jet centerline trajectory is rapidly bent over by the crossflow; in this region there is a substantial increase in the transverse scale of the jet due to turbulent entrainment, and the geometry of the cross-section of the jet changes to a kidney-shape (Needham *et al.*, 1992; Coelho and Hunt, 1992).

Though crossflows are often density stratified, the effects of stratification on jets in a crossflow have been much less studied. The object of this paper is to present the results of laboratory experiments on jets in a stratified crossflow, and in particular to report on the dependence of the length of the potential core on the buoyancy frequency N, the jet diameter and velocity D and U_J, and crossflow velocity U_∞. The observations and experimental studies of Fay *et al.* (1970), Hewett *et al.* (1971), Wright (1984) and Hunter (1993) provide results of jet centerline trajectory in a stratified crossflow. Principal results are that the trajectory of a jet in a stratified crossflow rises to a maximum height z_m, but subsequently falls to an equilibrium level z_e. That is, the trajectory evolves non-monotonically. However, knowledge of the details of the dynamics are poor as was shown by the numerical simulations of Zhang and Ghoniem (1994) and Hwang *et al.* (1995). Their numerical results confirmed the evolution of the trajectory but also showed the complexity of the vorticity field. In Section 2 the buoyancy and momentum length scales are discussed and an integral model is introduced to help analyze the results. After describing the experimental set-up and apparatus in Section 3, the results and discussion are presented in Section 4, with the conclusions following in Section 5.

2. LENGTH SCALES

A number of parameters characterize the flow (see Fig. 1). The jet discharge is characterized by the mass

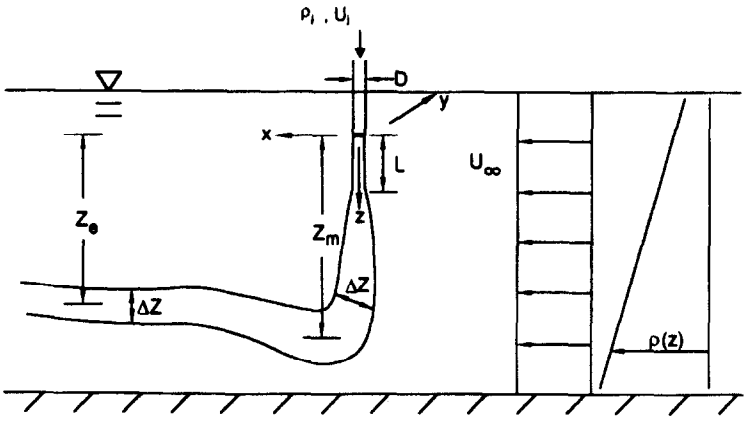

Fig. 1. Flow configuration and coordinate system of a transverse, circular jet in a density stratified crossflow.

flux $Q = (\pi/4)D^2U_J$, momentum flux $M = (\rho_J/\rho_A)U_JQ$ and buoyancy flux $B = g'Q$ where D is the jet diameter; U_J and ρ_J are the discharge velocity and density of the jet; ρ_A is the ambient crossflow density at the level of the jet exit; and $g'_0 = g(\rho_A - \rho_J)/\rho_A$. is the reduced gravitational acceleration. The crossflow is characterized by the magnitude of its velocity U_∞ and stratification $N = (-g/\rho\partial\rho/\partial z)^{1/2}$.

Wright (1984) derived various length scales to describe buoyancy, momentum and drag forces, and turbulent entrainment between the jet and the crossflow. For the purpose of describing the present experimental results it is convenient to define the following length scales. Buoyancy and momentum length scales l_B, l_M are defined by $l_B = B/U_\infty^3$, $l_M = M^{1/2}/U_\infty$. where l_B reflects the ratio of buoyancy and inertial forces, and l_M reflects the relative strength of the jet and crossflow velocities. A longitudinal length scale l_A over which stratification effects are significant is given by $l_A = U_\infty/N$: a vertical length scale describing the height of rise for a buoyant jet in a stratified fluid without a crossflow is $l_V = (B/N^3)^{1/4}$. For the range of parameters of the experiments (see Section 3 and Table 1) $l_M > l_B$, $l_M > l_V$ so that the flow field is momentum dominated close to the jet exit (i.e., the near field). Thus maximum rise heights z_m scale on l_m, and following Wright (1984), for a momentum dominated flow

$$\frac{z_m}{l_M} = K_1\left(\frac{l_A}{l_M}\right)^{1/2}. \tag{1}$$

Far from the jet exit for distances $x \gg l_M$, $x \gg l_B$ where buoyancy dominates, the equilibrium level z_e is

$$\frac{z_e}{l_B} = K_2\left(\frac{l_A}{l_B}\right)^{2/3}. \tag{2}$$

Wright (1984) determined the value of the constants K_1, K_2 from experiments and found $K_1 = 2.8$ and $K_2 = 1.88$.

Integral models have successfully predicted trajectory and evolution of jets in stratified crossflows (Slawson and Csanady, 1971; Briggs, 1975; Schatzmann, 1979; Davidson, 1989). Such models balance differential conservation equations of mass, momentum and energy. Typically, the conservation equations are simplified by the use of the Boussinesq approximation, and an entrainment hypothesis. The simple integral model of Slawson and Csanady (1971), which is also described by Davidson (1989), yields analytical predictions of the height z_c of the jet centerline and jet radius R as a function of distance x while the trajectory is still rising (see Fig. 1). The model of Briggs (1975) is similar. Schatzmann's (1979) model differs in that it invokes complex entrainment and drag formulations, and requires the specification of more empirical constants. Davidson's (1989) model by involving the added mass approach of Escudier and Maxworthy (1973) successfully predicts both the evolution of trajectory and dilutions. I use the model of Slawson and Csanady (1971) to help identify some principal features of the trajectory of a jet in a stratified crossflow.

$$z_c(x) = \left\{\frac{3B}{U_\infty\beta^2N^2}\left(1 - \cos\frac{Nx}{U_\infty}\right) + \frac{3M}{U_\infty\beta^2N}\sin\frac{Nx}{U_\infty} + \left(\frac{R_0}{\beta}\right)^3\right\}^{1/3} - \frac{R_0}{\beta} \tag{3}$$

$$R(x) = R_0 + \beta z_c(x) \tag{4}$$

In (3) the first term on the right-hand side involves the buoyancy flux B; the second term involves the initial momentum flux M, and the third and fourth terms involve the virtual jet radius R_0 which is taken as $R_0 = R_s(U_J/U_\infty\rho_J/\rho_A)^{1/2}$ with R_s the jet exit radius. β is an empirical coefficient that describes the growth of the jet due to turbulent entrainment by relating the change in jet radius linearly to the change in height of the centerline of the jet. Note that for a flow with

negligible momentum (i.e., a plume) for small values of Nx/U_∞ when stratification effects can be expected to be small, the first term on the right-hand side of (3) yields the well-known two-thirds law ($z_e \sim x^{2/3}$) for plume rise under neutral stratification. Plumes in stably stratified environments do not rise indefinitely and (3) shows that the maximum rise occurs at $Nx/U_\infty = \pi$. For flows with negligible momentum the first term also suggests that the asymptotic equilibrium level z_e, which is of the same order as the maximum rise, can be considered as

$$z_e = \left(\frac{3B}{\beta^2 U_\infty N^2}\right)^{1/3}. \tag{5}$$

Briggs' (1975) survey gives the value of $\beta = 0.37$. The scaling arguments relate to the integral model (3) as a rearrangement of (2) shows that $z_e \sim (B/U_\infty N^2)^{1/3}$. In the results to follow I check that the prediction of (3) of the maximum rise occurring at $Nx/U_\infty \approx \pi$, and that the scaling arguments describe maximum and equilibrium rise heights in accord with (1) and (2).

3. EXPERIMENTAL SET-UP

The experiments were performed in a water tunnel which was capable of driving a moving fluid column of linear density profile with a uniform velocity profile (see Fig. 1). The test section is 160 cm long, 22 cm high and 20 cm wide and possesses a free surface to facilitate the introduction of probes. The stratified water column is driven by a pump of the design of Kovasznay (1971). Briefly, two series of thin circular disks, vertically stacked and co-rotating, drives the stratified fluid column at speeds up to 5 cm s^{-1} without appreciably mixing the stratified fluid column. The density profile did not change measurably over the duration of an experiment. Linear density profiles were generated by salinity differences using the two-tank method of Oster (1965): this procedure took a period of 12 h for each filling of the water tunnel. A typical density profile is shown in Fig. 2 where it is evident that the density profile is linear except near the top surface and bottom boundary. Mean velocities in the stratified water tunnel are uniform aside from boundary layers which were approximately 1 cm thick at the side and bottom boundaries. (Free stream turbulence levels of the crossflow were less than 0.3% of its mean velocity U_∞.)

The jet exited from a circular steel pipe of internal diameter $D = 0.2$ cm. The steel pipe, which was rigidly mounted to eliminate vibration, was aligned vertically, perpendicular to the stratified crossflow. The jet exit was located 1 cm below the top water level of 19.4 cm. A combination of a second pump and a valve was used to regulate the supply to the jet from a storage reservoir of brine of density ρ_J to an accuracy of 5%. To avoid double diffusive effects the temperature difference between the fluid of the jet reservoir and water tunnel were carefully monitored and kept at less than 0.1°C.

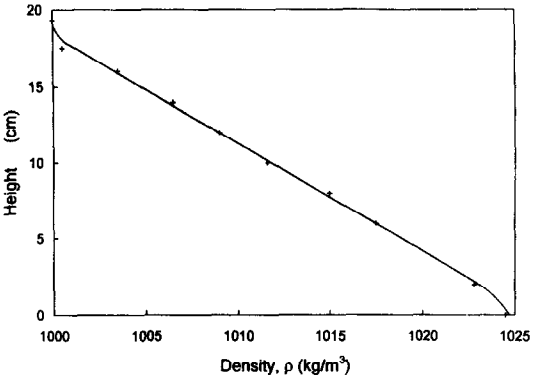

Fig. 2. Typical density profile. Data for Run 1 for which buoyancy frequency, N, of linear density gradient profile has a value of 1.17 s^{-1}.

Methylene blue dye was added to the jet reservoir to visualize the flow field. Simultaneous plan (x–y plane) and elevation (x–z plane) views, obtained by the use of a mirror positioned at 45° over the test section, were photographed by a motor-driven camera operating at a shutter speed of 1/125 s. Grids of 5 cm and 20 cm marked on the bottom and sidewalls of the water tunnel facilitated scaling of the jet trajectory and evolution from photographs and slides.

Mean density measurements were obtained by selective withdrawal of fluid samples with hypodermic tubing of 0.1 cm internal diameter, and then measuring the sample densities with an optical refractometer. Mean velocities were determined by tracking the traces of fine potassium permanganate ($KMnO_4$) crystals which had been dropped into the test section. For all experiments the depth, H, of the stratified fluid column was 19.4 cm. Values of the jet Reynolds number $U_J D/\nu$ varied from 1300 to 2600: values of the Reynolds number based on the crossflow velocity $U_\infty D/\nu$ varied between 40 and 78. Values of the experimental parameters of the buoyancy frequency N, source mass flux Q, jet exit velocity U_J, crossflow velocity U_∞, velocity ratio α, buoyancy and momentum fluxes B and M, length scales, l_B, l_V, l_M, l_A are given in Table 1.

4. RESULTS

4.1. *Visualization*

Figure 3 is a typical visualization of the elevation (x–z plane) and plan (x–y plane) views of the flow field of a jet in a stratified crossflow. The elevation view of Fig. 3a shows that the width of the jet is constant for a distance of approximately 10D in this case from the jet exit: this region is the potential core. (It is demonstrated later in Figs 10 and 11 that the potential core length varies, and depends on the value of the velocity and frequency ratio U_J/U_∞ and ND/U_∞.) For

Table 1

Run	N (s^{-1})	Q ($cm^3 s^{-1}$)	U_j ($cm\,s^{-1}$)	U_∞ ($cm\,s^{-1}$)	α	$\Delta\rho/\rho$	B ($cm^4 s^{-3}$)	M ($cm^4 s^{-2}$)	l_B (cm)	l_M (cm)	l_A (cm)	l_V (cm)	l_V/l_B
1	1.17	2.85	90.8	3	30.3	0.01149	32.13	261.75	1.190	5.393	2.564	2.116	1.78
2	1.01	3.33	106.1	2	53.1	0.00897	29.30	356.48	3.663	9.440	1.980	2.309	0.63
3	0.99	2.08	66.2	3	22.1	0.00600	12.24	138.52	0.453	3.923	3.030	1.885	4.16
4	0.93	2.22	70.7	3.9	18.1	0.00747	16.27	158.13	0.274	3.224	4.194	2.121	7.74
5	0.92	4.1	130.6	3	43.5	0.00600	24.13	538.67	0.894	7.736	3.261	2.359	2.64
6	0.85	3.1	98.7	2	49.4	0.00570	17.34	307.71	2.168	8.771	2.353	2.305	1.06
7	0.85	2.22	70.7	3.9	18.1	0.00596	12.98	157.89	0.219	3.222	4.588	2.144	9.79

Notes: Parameters are for run numbers for which trajectory information is presented in Figs 3–9.
$\alpha = U_j/U_\infty$, $\Delta\rho/\rho = (\rho_j - \rho_A)/\rho_A$, $g_0' = g(\Delta\rho/\rho)$, $B = g_0'Q$, $M = (\rho_j/\rho_A)\,U_jQ$, $l_B = B/U_\infty^3$, $l_M = M^{1/2}/U_\infty$, $l_V = (B/N^3)^{1/4}$, $l_A = U_\infty/N$.

distances beyond 10D the width of the jet grows due to entrainment and mixing. The trajectory of the centerline of the jet z_c can be seen to reach a maximum height of rise, z_m, and then to decrease to reach an equilibrium level z_e. The maximum thickness, Δz, occurs in the vicinity of the maximum rise, and attains a steady, but smaller value for distances beyond the location of the maximum rise. The boundary or edges of the jet trajectory are convoluted indicating turbulent mixing up to the maximum rise z_m; but for distances Nx/U_∞ beyond z_m the edges are much less convoluted. This suggests significant rates of entrainment and mixing up to z_m, and much reduced entrainment and mixing rates beyond z_m.

In previous studies there is little data of flow characteristics in the horizontal (i.e. $x - y$) plane. Here, close to the jet exit the plan view of Fig. 3b shows that the width of the jet is small: further from the exit, the width of the jet grows approximately linearly at 22°. This spreading angle is much greater than the spreading angles (3–7°) for jets in a crossflow in the absence of density stratification (Huq and Dhanak, 1996). This suggests that horizontal spreading is greater for the case of a stratified crossflow. The edges of the jet are convoluted for all distances with the scale of (horizontal) convolutions growing with distance, whereas in contrast, in the elevation view (vertical) convolutions diminish beyond z_m.

The visualizations of Figs 3 and 10 indicate that the salient features of jets in stratified crossflows are the existence of a potential core of variable length in the vicinity of the jet exit; a trajectory to a maximum height of rise, and subsequent relaxation to a lower equilibrium level; significant vertical and horizontal mixing up to the maximum height of rise, and only significant horizontal mixing beyond. In contrast, for jets in unstratified crossflows the variability of the potential core length is less (see Fig. 11a), the rise of the trajectory monotonic and the mixing more isotropic (Huq and Stewart, 1996).

4.2. *Trajectory and geometry*

The non-dimensional evolution of the jet centerline with distance is shown in Fig. 4. Here the data have been non-dimensionalized in the same manner as Hunter (1993) to facilitate comparison with his results. (The scaling arises from $z_e \sim (B/U_\infty N^2)^{1/3}$ see equations (2) and (3).) The trajectory rises steeply for $Nx/U_\infty < 2$ when stratification effects are small. For all runs the maximum height of rise z_m occurs at $Nx/U_\infty \approx \pi$ in accord with equation (3). The maximum dimensionless heights of rise of the present experiment are greater than the data of Hunter (1993) because the relative magnitude of the momentum flux of the present experiment is greater. (Recall that the prediction of the maximum rise from (3) has a contribution from the momentum flux.) For the present experiment the ratio of the momentum length scale l_M to buoyancy lengthscale l_B vary as $2.6 < l_M/l_B < 14.7$. In comparison for the experiments of Hunter

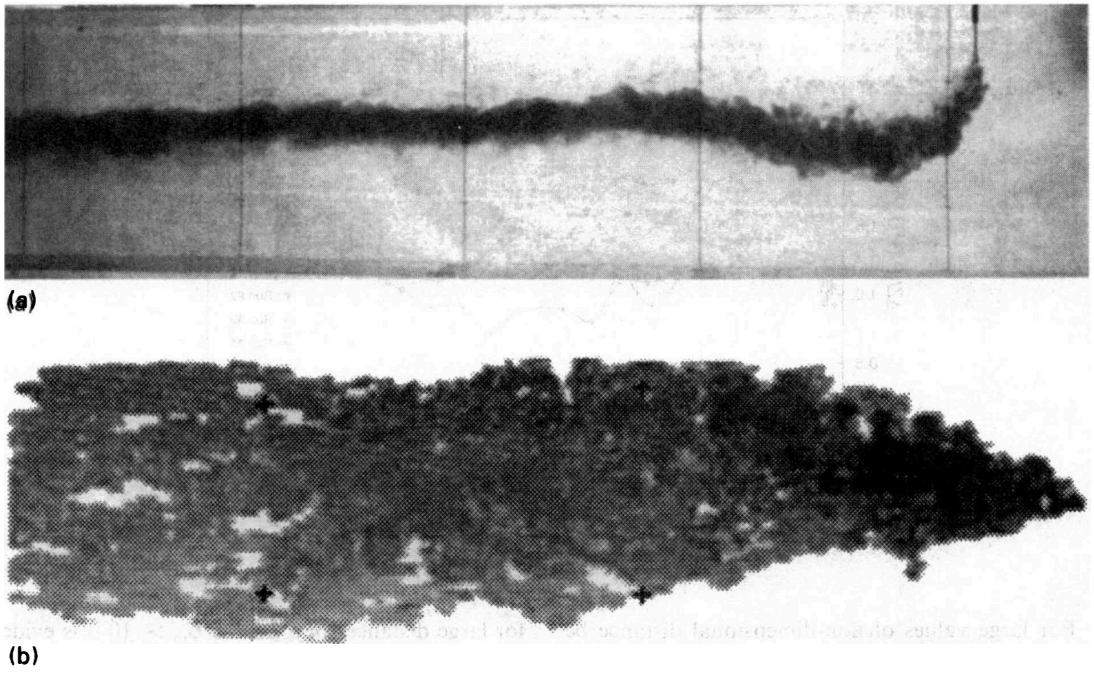

Fig. 3. Visualization showing (a) elevation view (x–z plane) of Run 3. Vertical lines are spaced 20 cm apart and (b) plan view (x–y) plane of Run 3. Crosses form a grid of 20 cm in the x direction, and 10 cm in the y direction.

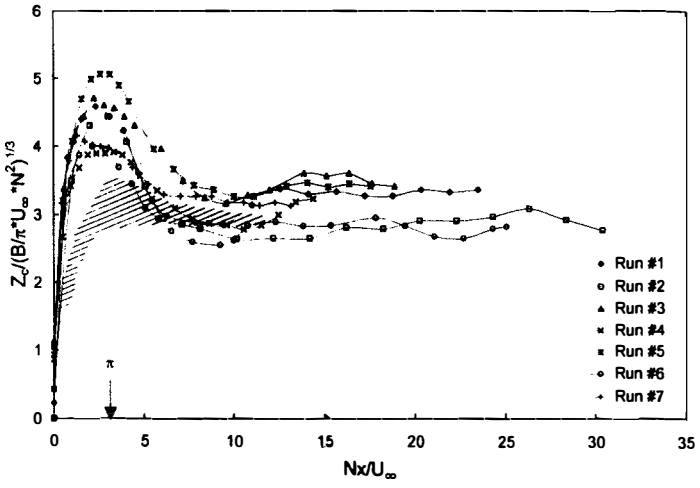

Fig. 4. Evolution of the trajectory of the centerline z_c of the jet with distance. Shaded region is data of Hunter (1993). Solid lines are best fit to data.

(1993) generally $l_M < l_B$, so that the flow in his experiment is buoyancy dominated.

The data of Fig. 4 also show that there is an overshoot of the trajectory. That is that values of z_c for large values of non-dimensional distance x are smaller than the values of z_m occurring at $Nx/U_\infty \approx \pi$. Values of the maximum rise shows considerable variability. For example, for Run 1 maximum non-dimensional value of z_c is about 5.0, whereas for Run 7 the maximum non-dimensional value is about 4.1. The data show a trend of larger maximum height of rise values for decreasing values of the length scale ratio l_V/l_B — values of l_V/l_B are 1.78 and 9.79 for Runs 1 and 7, respectively. The dependence of z_m upon l_V/l_B, also noted previously by Hunter (1993), arises because the ratio l_V/l_B characterizes whether the trajectory has been significantly bent over by the crossflow before its maximum rise is reached: larger values of the ratio l_V/l_B require larger crossflow velocities U_∞ so that the trajectories are relatively more bent over.

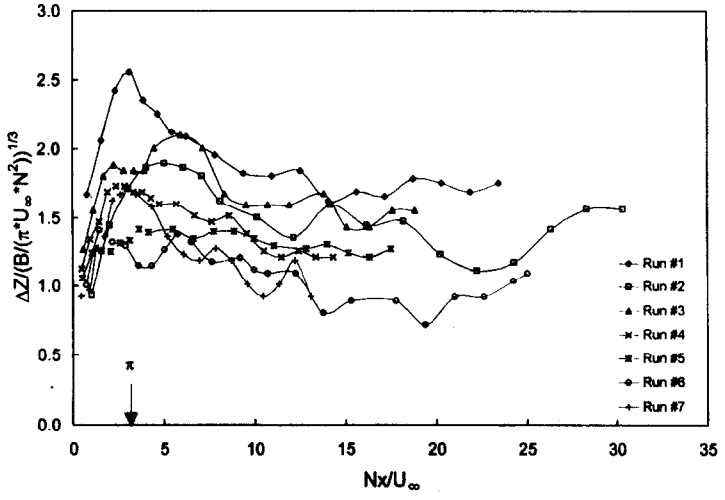

Fig. 5. Evolution of the jet thickness Δz with distance. Solid lines are best fit to data.

For large values of non-dimensional distance beyond the overshoot at $Nx/U_\infty \approx \pi$, all trajectories attain an equilibrium value of non-dimensional height $(\pi U_\infty N^2)^{1/3} z_c/B^{1/3} \approx 3.1 \pm 0.4$; this result is also in agreement with the observations of Hunter (1993).

The evolution of the vertical width Δz is similar to the evolution of the centerline trajectory. Figure 5 shows that for small distances $Nx/U_\infty < \pi$, non-dimensional values of thickness $(\pi U_\infty N^2)^{1/3} \Delta z/B^{1/3}$ increase rapidly as stratification effects are small and vertical and horizontal entrainment and mixing rates large. Thus it may be anticipated that the assumption of linear growth of the transverse scale (see equation (4)) of the integral model of Section 2 is most valid in this region. Maximum values of non-dimensional thickness occur at approximately $Nx/U_\infty \approx \pi$ with $(\pi U_\infty N^2)^{1/3} \Delta z/B^{1/3} = 2.5$, 1.7 for Runs 1 and 7 respectively. As for the centerline trajectory, thicknesses are also dependent upon the ratio l_V/l_B. For each run for large distances beyond $Nx/U_\infty > 10$ it is evident that the thickness is approximately constant with the value of non-dimensional thickness being approximately 80% of the maximum value of non-dimensional thickness at $Nx/U_\infty \approx \pi$: this is in accord with the prediction $z_E/z_M = 0.84$ of the integral model of Hewett *et al.* (1971) and Weil (1988).

Data for the evolution of the non-dimensional width of the jet for Runs 1 and 3 are presented in Fig. 6. The evolution of the width are typical of all runs and show that the width increases rapidly for small values of Nx/U_∞. Unlike the trajectory z_c and thickness Δz for which maxima occur at $Nx/U_\infty \approx \pi$, widths increase rapidly up to $Nx/U_\infty \sim 7$. Beyond $Nx/U_\infty > 7$ widths continue to increase albeit more gradually. Though initially widths and thicknesses are similar in magnitude, for distances beyond $Nx/U_\infty \sim \pi/2$ the width exceeds the thickness of the jet. This is consistent with the interpretation of the

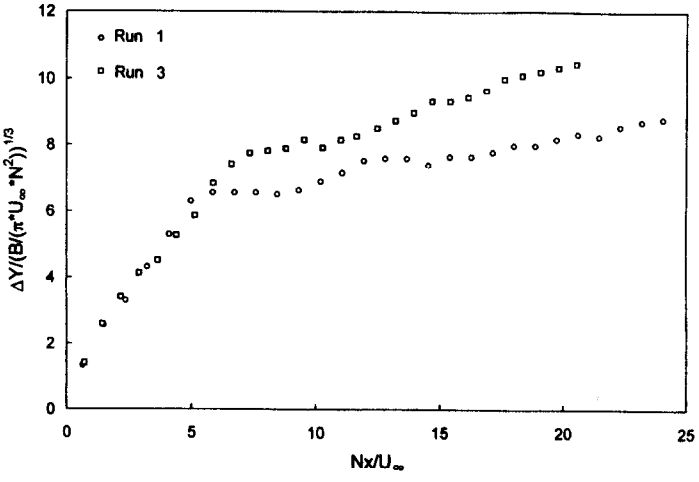

Fig. 6. Evolution of the jet width Δy with distance.

visualizations of Fig. 3 that a principal effect of stratification is to eventually suppress vertical motions and scales, and that for large distances when effects of stratification are pronounced, the spreading of the jet is predominantly horizontal. Estimates of the entrainment coefficient β were calculated by utilizing (4) from measured values of the height z_c, thickness Δz, and width Δy at $Nx/U_\infty = 1.5$ for Runs 1 and 3. Thickness measurements gave a value of $\beta = 0.40$ whereas width measurements yielded $\beta = 0.62$. That the value of the entrainment coefficient varies by 50% suggests that caution be exercised to select the appropriate value of β for the chosen transverse scale (either Δz or Δy) for jets in stratified crossflows. In comparison it should be noted that for buoyant plumes in a homogeneous crossflow Huq and Stewart (1996) found that values of entrainment coefficients based on Δy were only 10% greater than coefficients based on Δz.

The geometry of the cross section of the jet is initially circular so that the value of the aspect ratio, defined as $\Delta y/\Delta z$, is unity. With increasing distance from the jet exit the interaction of the jet and the crossflow bends the jet trajectory and distorts the jet cross section (Needham *et al.*, 1988; Coelho and Hunt, 1992; Huq and Dhanak, 1996). For the buoyant jet in a crossflow of homogeneous density Huq and Stewart (1996) found that values of the aspect ratio evolved from unity to about 1.3 for very large distances from the jet exit. Here, for the jet in a stratified crossflow, Fig. 7 shows that values of the aspect ratio, which were determined by best-fit curves to non-dimensional widths and thicknesses of Figs 5, 6, are similar to that for the buoyant jet in a homogeneous crossflow only up to the location of the maximum rise (z_m) of the jet trajectory at $Nx/U_\infty \sim \pi$. For distances beyond the location of the maximum rise, as vertical scales are inhibited by the effects of density stratification, and thicknesses diminish, the aspect ratio increases quickly to large values (> 5) and continues to increase. Thus, the geometry of the jet cross section is one of an ellipse that is increasingly vertical thin and horizontally broad. Physically, the increase in the value of the aspect ratio arises because as the jet approaches the equilibrium level vertical mixing and growth of the vertical thickness Δz are attenuated by stratification; whereas, in contrast horizontal growth is uninhibited – a situation similar to the collapse of a wake in a stratified fluid column.

4.3. *Maximum rise and equilibrium heights*

To check the validity of the scaling of Section 2, comparisons are made between measurements and predictions of the maximum height of rise z_m and the equilibrium (or terminal) level of the jet trajectory z_e. Recall that for the momentum dominated flow in the vicinity of the jet exit $(z_m/l_M) = K_1(l_A/l_M)^{1/2}$ and that for a buoyancy dominated flow far from the jet exit $z_e/l_B = K_2(l_A/l_B)^{2/3}$. Figure 8a shows that the present data for non-dimensional maxima of height of rise does indeed collapse as $(l_A/l_M)^{1/2}$ with a best-fit value

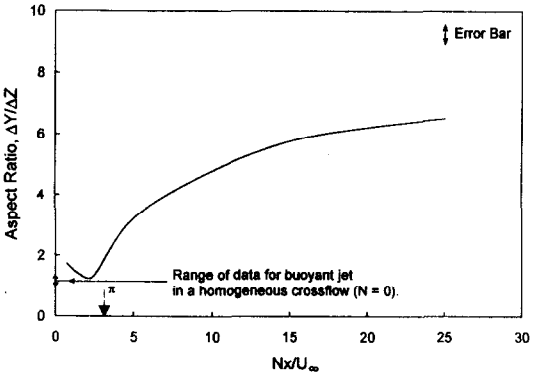

Fig. 7. Evolution of the aspect ratio $\Delta y/\Delta z$ of the jet with distance. Note that range of data for buoyant jets in a homogeneous crossflow is limited between 1 and 1.3 (Huq and Stewart, 1996).

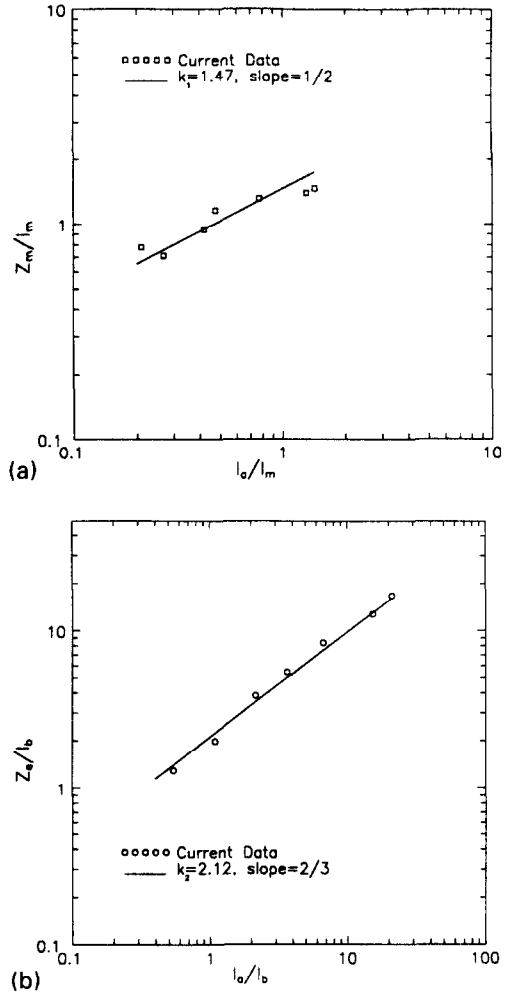

Fig. 8. Dependence of the (a) maximum height of rise z_m, on the ratio of length scales l_A/l_m. Line through data has a slope of 1/2, and the value of the coefficient K_1 in equation (1) is 1.47 and (b) equilibrium height of rise, z_e, on the ratio of length scales l_A/l_B. Line through data has a slope of 2/3, and the value of the coefficient K_2 in equation (2) is 2.12.

of the constant of proportionality $K_1 = 1.47$. This compares with the average value of $K_1 = 2.8$ for the experiments of Wright (1984). In fact, Wright (1984) noted that the value of K_1 varies with the ratio of length scales l_Q/l_M (see his Fig. 12) in his experiments. l_Q is defined as $Q/M^{1/2}$. For flows with $l_Q/l_M \to 0$ the relative effect of the crossflow is small (i.e. $U_\infty/U_J \to 0$). Conversely, increasing values of l_Q/l_M increases the relative effect of U_∞. For the present experiments $0.02 \leqslant l_Q/l_M \leqslant 0.05$; and the data in conjunction with Fig. 12 of Wright (1984) shows that K_1 depends on l_Q/l_M as $K_1 = 0.75(l_Q/l_M)^{-0.25}$.

The data for the non-dimensional equilibrium level of Fig. 8b show that $(z_e/l_B) \sim (l_A/l_B)^{2/3}$ also in agreement with integral model predictions. The value of the constant of proportionality $K_2 = 2.12$ compares with $K_2 = 2.6$ suggested by Briggs (1975) for buoyant plumes. The difference arises from the significant momentum flux of the present experiments. As shown by Hewett *et al.* (1971) this causes a significant portion of the trajectory to be momentum dominated with the consequence that the equilibrium level z_e described by (2) is too large.

Comparison of the equilibrium height z_e between predictions and measurements in conjunction with equation (5) also yields a value of the entrainment constant β in the integral model. Figure 9 shows that the agreement between predictions and the current data is good for a value of the entrainment parameter $\beta = 0.54$: this compares with the (average) value of $\beta = 0.37$ found by Briggs (1975) from a survey of available data, and also the value of $\beta = 0.40$ obtained by using (4) and present measured values of thickness Δz. As β is an entrainment coefficient it is natural to determine the value of β from the growth of the vertical scale of the jet. However, the data of Fig. 5 show that the vertical width Δz increases only for distances up to $Nx/U_\infty < \pi$. This suggests that the use of (5) to determine β is invalid. Rather the correct approach to determining β is to relate measurements of the vertical thickness Δz to z_c and using (4) to obtain the value of the coefficient as was done in Section 4.2.

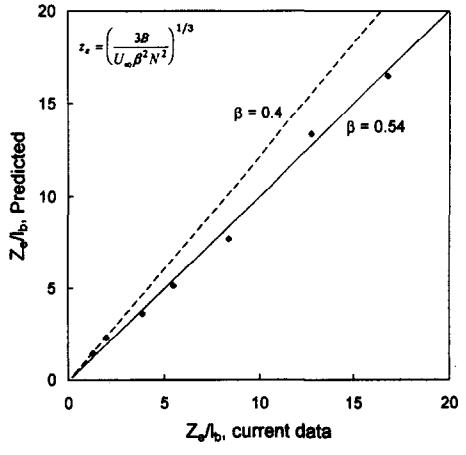

Fig. 9. Comparison of equilibrium height of rise, z_e with predictions given by $z_e = 3B/(U_\infty \beta^2 N^2)^{1/3}$. Dashed line $\beta = 0.4$; solid line $\beta = 0.54$.

4.4. *Variability of potential core length*

Detailed examination of the visualization of the flow in the vicinity of the jet exit showed considerable variation in the length of the potential core as a function of the parameters $\alpha = U_J/U_\infty$ and ND/U_∞. Figure 10 shows examples of such visualizations. Figure 10a is an example of a flow field with a short potential core length. Clearly, the jet is turbulent within a short distance of the exit. The length of the potential core in the flow field of Fig. 10b is strikingly longer. Eventually in both visualizations there is a rapid growth in the transverse dimension (Δz) of the jet flow field due to turbulent entrainment and mixing. The outer edges of the jets in Figs 10a, and b, which are interfaces between the rotational flow within the jet and irrotational flow of the laminar crossflow, are convoluted, with the largest scale of the convolutions being up to approximately 25% of the local transverse dimension.

Data for the lengths of the potential core for all experiments are shown in Fig. 11. The lengths of the potential core for the case of a jet in a crossflow in the absence of density variations (i.e., the density of the jet is the same as that of the homogeneous crossflow) is compared with the results of Pratte and Baines (1967) in Fig. 11a. The abscissa in Fig. 11a is the ratio, α, of the jet exit velocity to crossflow velocity, and the ordinate is the length of the potential core non-dimensionalized by the jet exit diameter. Over the range of values of α of the experiments ($18 < \alpha < 53$, see Table 1) the present results of $L/D \approx 5.7$ can be seen to be in approximate accord with the results of Pratte and Baines. (Note that the data of Pratte and Baines is well described by the empirical formula $L/D = 6.2 \exp(-3.3\bar{U}/w_s)$ (Fan, 1967; Alton *et al.*, 1993).)

Data for the length of potential core for jets in a stratified crossflow are presented in Fig. 11b. Here the abscissa, ND/U_∞, is a ratio of frequencies N and U_∞/D formed from the independent variables N, D, U_∞ (see Fig. 1). Data for the case in the absence of density variations for all values of α coincide at $ND/U_\infty = 0$: for stratified crossflows i.e. $ND/U_\infty > 0$ it is evident that non-dimensional potential core lengths L/D can be greater ($L/D \approx 25$) or smaller ($L/D \approx 3$) than potential core lengths in the absence of density variations where ($L/D \approx 5.7$). Best-fit parabolas drawn through the data points show the dependence of L/D upon the value of α — with larger values of L/D for increasing values of α for a given value of ND/U_∞.

The effect of increasing α is to reduce the intensity of the crossflow so that the jet trajectory bends over more slowly. This is seen more formally by considering jet stiffness. Jet stiffness is defined as the ratio of the jet discharge momentum flux to the drag force of

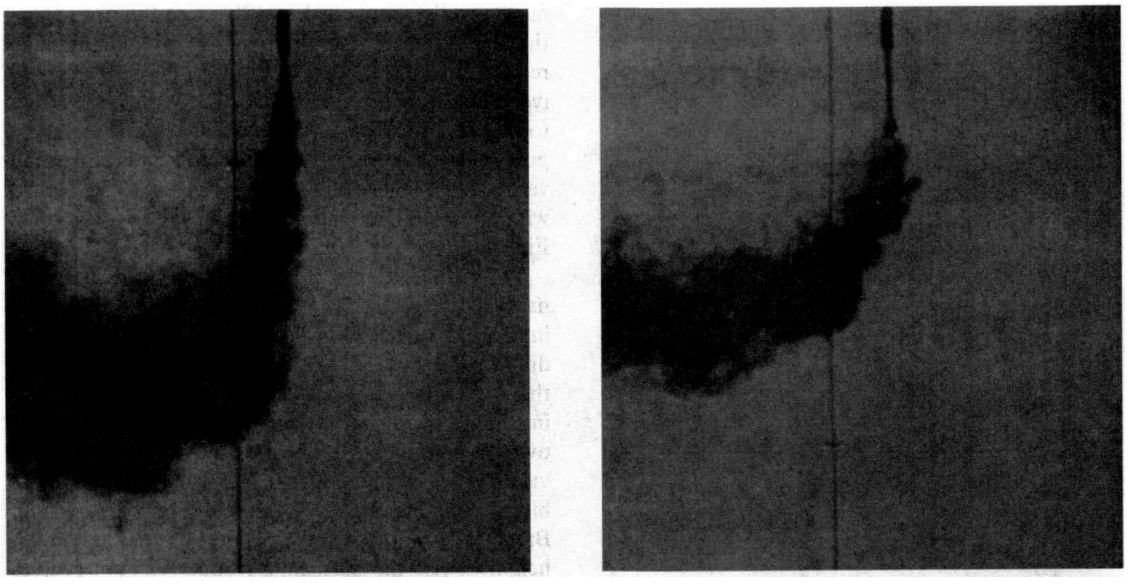

a b

Fig. 10. Elevation views (x–z plane) showing detail in vicinity of jet exit. The circular pipe of the jet is visible near the upper edge. For (a), the jet of Run 1 becomes turbulent very close to the exit (i.e. a short potential core length). In (b), the potential core length of Run 3 is longer, and the jet does not become unstable till further from the exit.

the crossflow on the potential core of the jet. The jet discharge momentum flux varies as DU_j^2 whereas the drag force varies as DU_∞^2 per unit length. Thus jet stiffness varies as $\alpha^2 = (U_j/U_\infty)^2$: presumably, potential core lengths will be greater for jets which are relatively more stiff.

The dependence of the core length, L/D, upon the ratio of frequencies ND/U_∞ is not monotonic. For weak stratification ($ND/U_\infty < 0.02$) the lengths of the potential core increase up to $L/D \approx 15$. Contrastingly, for larger values of ND/U_∞ potential core lengths can be shorter than in the absence of density variations. For all values of α the non-dimensional length of the potential core L/D increases initially for increasing values of ND/U_∞. In contrast, for sufficiently large values of ND/U_∞ values of L/D decrease with increasing values of ND/U_∞ for all values of α. The onset of the location of the inverse dependence of L/D on ND/U_∞ varies with α. For example, for $\alpha = 20$, L/D decreases for $ND/U_\infty > 0.03$; for $\alpha = 30$, L/D decreases for $ND/U_\infty > 0.06$; for $\alpha = 50$, L/D decreases for $ND/U_\infty > 0.08$. For the present purpose of qualitative description, the following is noted: resonance will promote instability when the vortex shedding frequency f of the crossflow past the potential core coincides with the frequency of internal waves capable of being supported in the stratified fluid column. There is presently no data on vortex shedding characteristics; however, for similar values of Reynolds numbers as in the present study for a jet in an unstratified crossflow Huq and Dhanak (1996) found the value of the Strouhal number $S_T = fD/U_\infty = 0.07$. Thus, $f \approx 0.07U_\infty/D$; for the present experiments the value of N/f, the ratio of buoyancy frequency N to vortex shedding frequency f varies between 0.55 and 1.26. This suggests that vortex shedding and resonance with internal waves are likely to be important in determining jet stability and potential core lengths. Note that the variability of the potential core length does not have a significant effect on the equilibrium value z_e of the trajectory as Figure 4 shows that $z_e(\pi U_\infty N^2)^{1/3}/B^{1/3} \approx 3.1 \pm 0.4$. for all trajectories regardless of potential core lengths.

4.5. *Dilution*

The bulk dilution which occurs at a given downstream distance is determined by calculating the volumetric flow rate of the jet and comparing it to the initial flow rate Q of the jet. The volumetric rate is taken to be as $\Delta y \Delta z U_\infty$: thus the ratio $\Delta y \Delta z U_\infty/Q$ yields an estimate of the dilution. (This should be understood to be an estimate because for small distances in the vicinity of the jet exit the use of U_∞ as a characteristic jet centerline velocity is likely to be an underestimate.) The evolution of dilution with non-dimensional distance Nx/U_∞ shown in Fig. 12a possesses distinctly different slopes for small and large distances. The data shows that dilution increases rapidly from unity to approximately 25 by $Nx/U_\infty \approx 6.5$; thereafter, for larger values of Nx/U_∞ dilution increases more slowly: for example, between $Nx/U_\infty = 6.5$ and 30 dilution only increases from 25 to about 30. The faster rate of increase of dilution for distances $Nx/U_\infty \leqslant 6.5$ can be attributed to

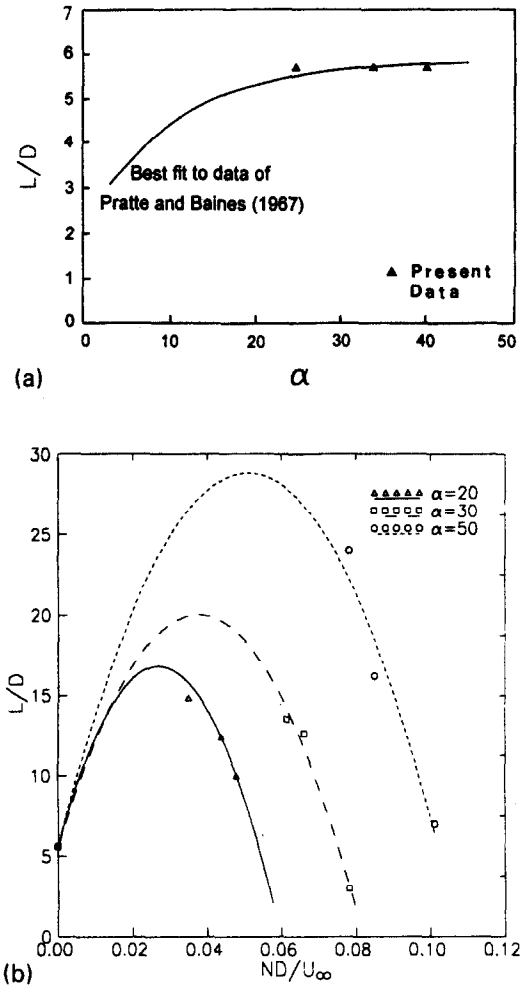

Fig. 11. Dependence of the potential core length L on the velocity ratio $\alpha = U_J/U_\infty$ (a) for jets in crossflow without density variations. Solid line is a best-fit to data of Pratte and Baines (1967) and (b) non-dimensional frequency ND/U_∞ for a jet in a density stratified crossflow. Lines are best-fit parabolas through data.

three-dimensional mixing and entrainment (see discussion of visualization of Sections 4.1 and 4.2) which occurs for $Nx/U_\infty \leqslant 6.5$. Noting that beyond $Nx/U_\infty > 6.5$ that the evolution of Δy also evolves more slowly (see Fig. 6) and that Δz values are constant (see Fig. 5), the slower rate of increase of dilution for large distances $Nx/U_\infty > 6.5$ can be understood to arise from the relatively inefficient process of horizontal (i.e., anisotropic) mixing.

Also evident in Fig. 12a is the faster increase in dilution for small distances $Nx/U_\infty < 6.5$ for jets with short potential cores. Examination of the visualization of Fig. 10 reveals that this is due to the earlier occurrence of instability and turbulent mixing for jets with shorter potential cores. For large distances beyond $Nx/U_\infty > 6.5$ values of dilution rates are not dependent on the length of the potential core. The attenuation of mixing rates beyond $Nx/U_\infty \approx 6.5$ is more vividly shown in Fig. 12b. Here the ordinate is the derivative of the ordinate of Fig. 12a and so reflects entrainment rates. The data show large positive values of entrainment rate $(\mathrm{d}/\mathrm{d}x)\,(\Delta y \Delta z U_\infty/Q)$ up to $Nx/U_\infty \sim 6$. For both jets with long and short potential cores entrainment rates diminish to small values for distances beyond $Nx/U_\infty = 6.5$ in accord with the slowly changing values of dilution of Fig. 12a.

The visualization of Fig. 13 shows evidence of a dynamical mechanism of mixing in the rapidly entraining region of the flow field in which there is rapid dilution (i.e. $Nx/U_\infty < 6.5$). Seen here in the vicinity of the maximum height of rise are backward breaking instabilities with amplitudes approximately half of the overall jet thickness. The form of the instability is visually similar to the Kelvin–Helmholtz (K–H) instability visualizations of Thorpe (1971) and Koop and Browand (1979). In the vicinity of the maximum height of rise the baroclinic torque $(\nabla p \times \nabla \rho)$ evolves rapidly so that the dynamical balances are complex (Zhang and Ghoniem, 1994). This is illustrated by the fact that $K - H$ instability does not always arise as Fig. 10 shows that for the parameters of Runs 1 and 3 the $K - H$ instability is absent in the vicinity of the maximum height of rise.

Measurements of the evolution of the mean density along the centerline of the jet trajectory were undertaken to confirm the diminution of dilution rates for large distances. Figure 14 shows the evolution of the density anomaly with distance. The non-dimensional density anomaly is defined as $(\rho_A - \rho_J)/(\rho_A - \rho_J)_{MAX}$ where ρ_J is the mean density at the jet centerline at a given z coordinate, and ρ_A is the mean ambient density of the crossflow (i.e., outside of the jet) at the same elevation; the denominator $(\rho_A - \rho_J)_{MAX}$ is the maximum value of the density difference $(\rho_A - \rho_J)$ at the jet exit. For reference the location of the mean density measurements (designated by the letters a–e) are indicated on the accompanying visualization. With distance from the jet exit the density anomaly generally decreases. At (a) the density anomaly has decreased to about 0.7 of the maximum occurring at the jet exit. At (b) the location of the maximum rise z_m the density anomaly is greater than 1.0 due to the overshoot of the jet trajectory. At (c) where $Nx/U_\infty \approx 6.5$ the density anomaly has decreased to 0.2: for locations (d) and (e) for which $Nx/U_\infty > 6.5$ the density anomaly is negligibly small. The slopes of the evolution of the density anomaly are large up to location (c); beyond (c) the slopes of the evolution of the density anomaly are markedly smaller, consistent with smaller entrainment rates. This is in accord with the interpretation of the visualizations of Section 4.1 that for small values of Nx/U_∞ up to the maximum height of rise both horizontal and vertical mixing occurs, but that for $Nx/U_\infty > 6.5$ there is only significant rates of horizontal mixing so that dilution rates are attenuated.

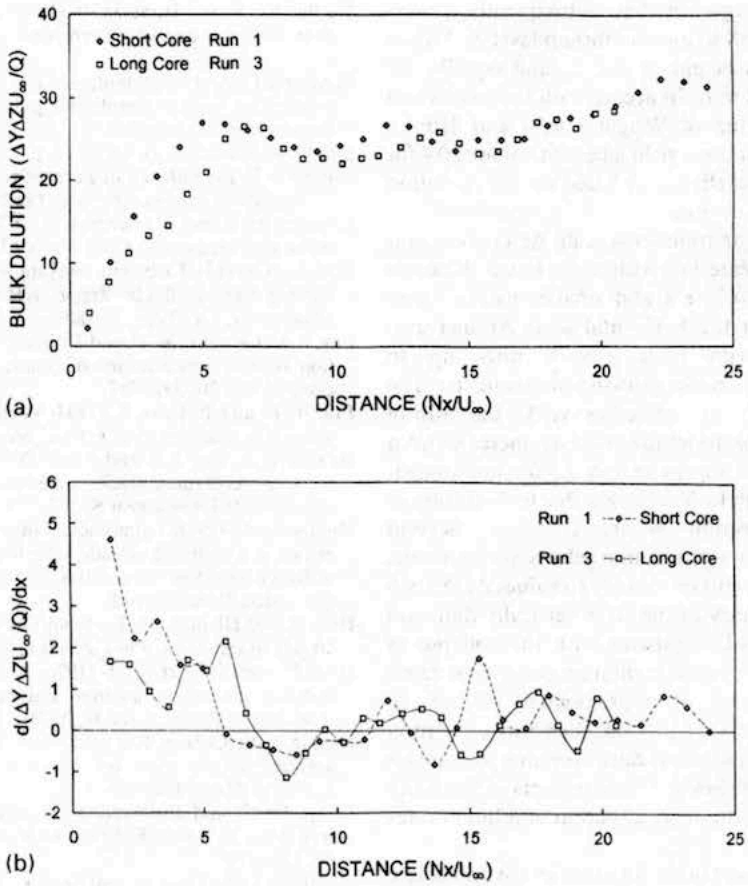

Fig. 12 Evolution of (a) volumetric bulk dilution with distance and (b) rate of change of volumetric bulk dilution with distance.

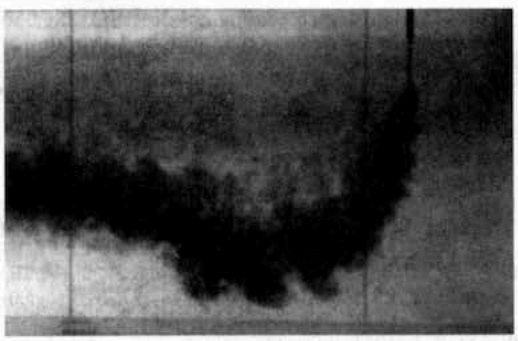

Fig. 13 Elevation view (x–z plane) showing detail of K-H instability in vicinity of maximum height of rise for Run 5.

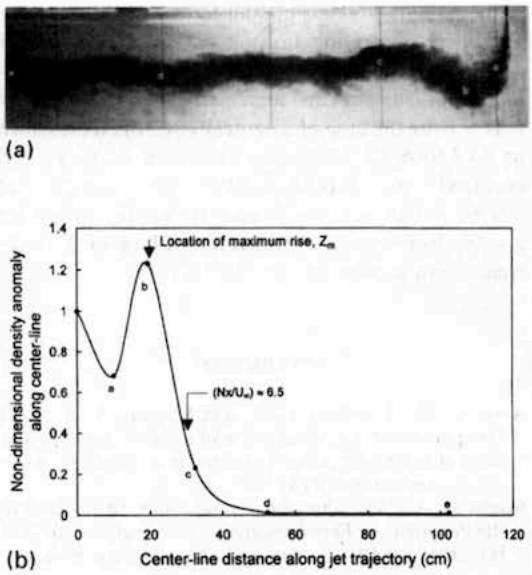

Fig. 14 (a) Elevation view (x–z plane) of Run 1. Letters a–e are locations where density measurements were undertaken. (b) Evolution of density anomaly $(\rho_A - \rho_J)/(\rho_A - \rho_J)_{MAX}$ with distance.

5. CONCLUSIONS

The results of an experimental study of a steady, circular jet in a steady, linearly stratified crossflow are described in this paper. Using flow visualization I found that the evolution of the trajectory of the jet centerline z_c rises quickly to reach a maximum value z_m at $Nx/U_\infty \approx \pi$. This is in good agreement with the

predictions of integral models. Subsequently, centerline trajectories fall to an equilibrium level z_e. Values of the maximum height of rise z_m and equilibrium level z_e are found to be in accord with the results and dimensional scaling of Wright (1984) and Hunter (1993); and correlations yield a best-fit value of 0.4 for the entrainment coefficient β based on the evolution of the vertical thickness.

The thickness or transverse scale Δz evolves similarly to the jet centerline with a maximum thickness occurring at $Nx/U_\infty \approx \pi$ and smaller values thereafter. In contrast the horizontal scale Δy increases monotonically with large growth rates up to $Nx/U_\infty = 6.5$ and smaller growth rates thereafter. The aspect ratio of the jet, defined as $\Delta y/\Delta z$, the ratio of the jet width Δy to the jet thickness Δz, increases from values of unity to approximately 1.5 for non-dimensional distances up to $Nx/U_\infty \approx \pi$ due to distortion of the jet cross section by the crossflow. Beyond $Nx/U_\infty \approx \pi$ when stratification effects predominate, the aspect ratio increases steadily to values $\Delta y/\Delta z > 6$ so that the geometry of the jet is vertically thin, and horizontally broad, consistent with the collapse of vertical mixing. Volumetric dilution rates show rapid increases to values of approximately 25 up to $Nx/U_\infty \approx 6.5$. For $Nx/U_\infty > 6.5$ when horizontal mixing predominates, dilution rates continue to increase albeit much more slowly. Measurements of the mean density field confirm the attenuation of dilution rates for $Nx/U_\infty > 6.5$.

The potential core of the jet exists in the immediate vicinity of the jet exit, and is where the transverse scale of the jet changes little. It is found that the length of the potential core varies with the velocity ratio $\alpha = U_J/U_\infty$, the ratio of jet and crossflow velocities, and non-dimensional frequencies ND/U_∞. The length of the potential core is greater for greater values of α. The effect of stratification on potential core lengths can be non-monotonic. For weak stratification potential core lengths can increase from the value of $L/D \approx 6$ for the case of a neutrally stratified crossflow up to $L/D \approx 25$. Maximum measured values of L/D occurred at $ND/U_\infty \approx 0.03$ for $\alpha = 20$; at $ND/U_\infty \approx 0.06$ for $\alpha = 30$ and at $ND/U_\infty \approx 0.08$ for $\alpha = 50$. For strong stratification values of L/D decrease with increasing values of ND/U_∞.

REFERENCES

Alton, B. W., Davidson, G. A. and Slawson, P. R. (1993) Comparison of measurements and integral model predictions of hot water plume behavior in a crossflow. *Atmospheric Environment* **27A**, 589.

Briggs, G. A. (1975) Plume rise predictions. In *Lectures on Air Pollution and Environmental Impact Analyses*, ed. D. A. Haughen, pp. 59–111. American Met. Society, Boston.

Coelho, S.L.V. and Hunt, J.C.R. (1989) The dynamics of the near field of strong jets in crossflows. *J. Fluid Mech.* **200**, 95.

Davidson, G. A. (1989) Simultaneous trajectory and dilution predictions from a simple integral model. *Atmospheric Environment* **23**, 341–349.

Eiff, O. S., Kawall, J. G. and Keffer, J. F. (1995) Lock-in of vortices in the wake of an elevated round turbulent jet in a crossflow. *Experiments Fluids* **19**, 203.

Escudier, M. P. and Maxworthy, T. (1973) On the motion of turbulent thermals. *J. Fluid Mech.* **61**, 541–552.

Fan, L. N. (1967) Turbulent buoyant jets into stratified or flowing ambient fluids. Report KH-R-15, W. M. Keck Laboratory, Cal. Tech., Pasadena, CA.

Fay, J. A., Escudier, M. P. and Hoult, D. P. (1970) A correlation of field observations of plume rise. *J. Air Pollut. Control Ass.* **20**, 391–397.

Fric, T. F. and Roshko, A. (1994) Vortical structure in the wake of a transverse jet. *J. Fluid Mech.* **279**, 1–47.

Hewett, T. A., Fay, J. A. and Hoult, D. P. (1971) Laboratory experiments of smokestack plumes in a stable atmosphere. *Atmospheric Environment* **5**, 767–789.

Hunter, G. C. (1993) Experimental investigation of a buoyant jet in a stratified crossflow. In *Waves and Turbulence in Stably Stratified Flows*, eds S. D. Mobbs and J. C. King. Clarendon Press, Oxford.

Huq, P. and Dhanak, M. R. (1996) The bifurcation of circular jets in crossflow. *Phys. Fluids* **8**, 754–763.

Huq, P. and Stewart, E. J. (1996) A laboratory study of buoyant plumes in laminar and turbulent crossflows. *Atmospheric Environment* **30**, 1225–1335.

Hwang, R. R., Chiang, T. P. and Yang, W. C. (1995) Effect of ambient stratification on buoyant jets in cross-flow. *J. Engng. Mech.* **121**, 865–872.

Koop, C. G. and Browand, F. K. (1979) Instability and turbulence in a stratified fluid with shear. *J. Fluid Mech.* **93**, 135–159.

Needham, D. J., Riley, N. and Smith, J. H. B. (1988) A jet in crossflow. *J. Fluid Mech.* **188**, 159.

Odell, G. M. and Kovasznay, L.S.G. (1971) A new type of water channel with density stratification. *J. Fluid Mech.* **50**, 535–545.

Oster, G. (1965) Density gradients. *Sci. Am.* **213**, 70.

Pratte, W. and Baines, W. D. (1967) Profiles of the round turbulent jets in a crossflow. *ASCE J. Hyd. Div.* **92**, 53–64.

Rajaratnam, N. (1976) *Turbulent Jets*. Elsevier, Amsterdam.

Schatzmann, M. (1979) An integral model of plume rise. *Atmospheric Environment* **13**, 721–731.

Slawson, P. R. and Csanady, G. T. (1971) The effects of atmospheric conditions on plume rise. *J. Fluid Mech.* **47**, 33-49.

Thorpe, S. A. (1971) Experiments on the instability of stratified shear flows: miscible fluids. *J. Fluid Mech.* **46**, 299–319.

Weil, J. C. (1988) Plume rise. In *Lectures on Air Pollution Modelling*, eds A. Venkatram and J. C. Wyngaard, pp. 119–166. American Met. Society, Boston.

Wright, S. J. (1984) Buoyant jets in density-stratified crossflow. *J. Hyd. Engng.* **110**, 643–656.

Zhang, X. and Ghoniem, A. F. (1994) A computational model for the rise and dispersion of wind-blown, buoyancy-driven plumes — II. Linearly stratified atmosphere. *Atmospheric Environment* **28**, 3005–3018.